

PCCP

Accepted Manuscript

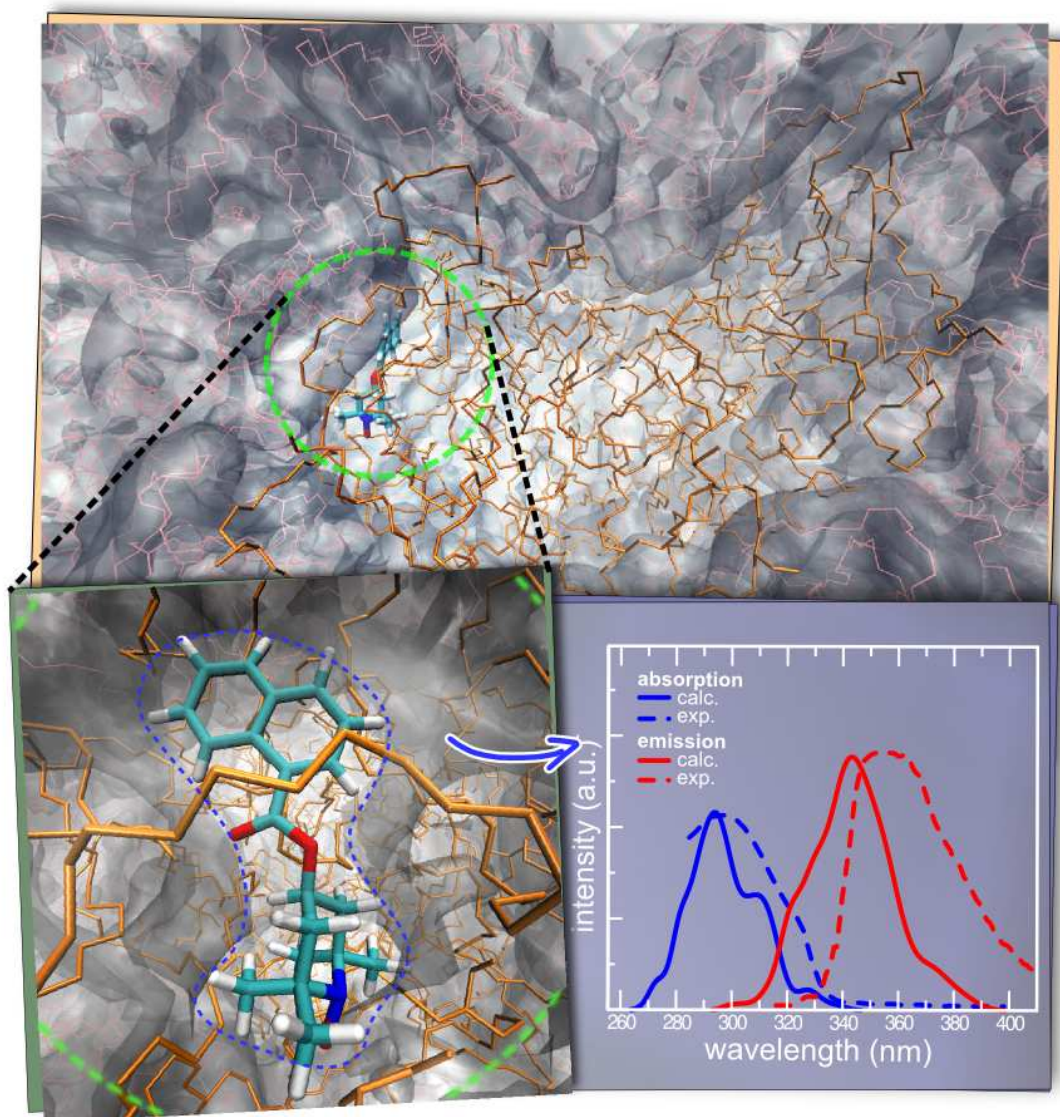


This is an *Accepted Manuscript*, which has been through the Royal Society of Chemistry peer review process and has been accepted for publication.

Accepted Manuscripts are published online shortly after acceptance, before technical editing, formatting and proof reading. Using this free service, authors can make their results available to the community, in citable form, before we publish the edited article. We will replace this *Accepted Manuscript* with the edited and formatted *Advance Article* as soon as it is available.

You can find more information about *Accepted Manuscripts* in the [Information for Authors](#).

Please note that technical editing may introduce minor changes to the text and/or graphics, which may alter content. The journal's standard [Terms & Conditions](#) and the [Ethical guidelines](#) still apply. In no event shall the Royal Society of Chemistry be held responsible for any errors or omissions in this *Accepted Manuscript* or any consequences arising from the use of any information it contains.



TOC Graphic: Structure, Dynamic and Photophysical Properties of a Fluorescent Dye Incorporated in an Amorphous Hydrophobic Polymer Bundle, by N. De Mitri, G. Prampolini, S. Monti, and V. Barone.

Structure, Dynamic and Photophysical Properties of a Fluorescent Dye Incorporated in an Amorphous Hydrophobic Polymer Bundle

N. De Mitri^a, G. Prampolini^{b,*}, S. Monti^{a,b}, and V. Barone^a

^a*Scuola Normale Superiore,*

piazza dei Cavalieri 7, I-56126 Pisa, Italy

^b*Istituto di Chimica dei Composti OrganoMetallici (ICCOM-CNR),*

Area della Ricerca, via G. Moruzzi 1, I-56124 Pisa, Italy

May 20, 2014

Abstract

The properties of a low molecular weight organic dye, namely 4-naphthoxy-1-methoxy-2,2,6,6-tetramethylpiperidine, covalently bound to an apolar polyolefin are investigated by means of a multi-level approach, combining classical molecular dynamics simulations, based on an purposely parameterized force fields, and quantum mechanical calculations, based on density functional theory (DFT) and its time-dependent extension (TD-DFT). The structure and dynamics of the dye in its embedding *medium* is analyzed and discussed in the light of the entangling effect of the surrounding polymer, also by comparing it to the results obtained for a different environment, *i.e.* toluene solution. The influence on photophysical properties of long lived cages, found in the polymeric embedding is eventually investigated in terms of slow and fast dye's internal dynamics, by comparing computed IR and UV spectra with their experimental counterparts.

*Corresponding author

1 Introduction

During the past few decades, the continuous progress in the design of nanohybrid materials has been inspired by the growing interest in creating new intelligent systems, with unique magnetic, electric, optical or mechanical properties, which could be modulated and controlled by means of appropriate external sources (light, heat, magnetic fields, etc.), for specific use in areas as diverse as aerospace, electronics, ceramics, packaging, molecular biology, biomedicine, drug delivering and targeting. Piezoelectric ceramics, electro-rheological fluids, nanoparticles, hydrogels, photo-catalysts and synthetic polymers, have long been classified as belonging to this class of materials. All of them can show characteristic responses to external perturbations, such as the aptitude to return to their original shape after plastic deformations, the tendency to change their color as a function of an electric field, and other more complex reactions. Due to these special properties, complex materials can be effectively viewed as versatile "smart" multichannel systems or mimetic machines to be used in multipurpose task devices¹⁻⁵ This is clearly reflected in the list of sources which could affect their behavior and performance, namely temperature, pH, chemical agents, solvent concentration, ionic strength, pressure, strength, electric/magnetic fields and different types of radiations. Polymeric substances are particularly suitable for these types of applications⁴ because they have the widest variety and range of mechanical and physico-chemical properties of all known materials.

The incorporation of photo-responsive chromophores into polymer matrices enables the creation of receptive compounds, sometimes referred to as "smart" polymers,⁶⁻¹¹ which could change their optical or electronic characteristics upon light irradiation. The integrated molecules could be dispersed inside the polymer matrices¹² or covalently bound to the chains of the polymers,^{13,14} thus determining specific responses, such as changes in size, shape and polarity,¹⁵ of the composite materials to the external stimuli. The dispersion of a dye inside a polymer is the simplest and one of the most cost-effective methods used today to obtain quickly heterogeneous composites, but the systems produced are thermally unstable and the inserted molecules could self-interact and aggregate into clusters. Instead, covalent functionalization can generate controlled architectures with known location and concentration of the bonded molecules, higher concentration

levels of the dyes and a reduced thermal relaxation of their alignments. However, the synthetic route required in this case is very elaborate and should be specifically defined for each polymer and dye.^{12,16,17} The structures of the resulting assemblies can be inferred from spectroscopic or kinetic measurements (distance dependencies of energy transfer, electron-transfer quenching, etc.)^{18,19} Among many different kinds of "smart" polymers, functionalized polyolefins have attracted a lot of attention, and their synthesis and application have been recently reviewed.^{20,21}

However, due to the complexity of the intramolecular and intermolecular interactions inside these systems it is difficult to disclose and identify precisely, from an experimental point of view, the factors responsible for the variation of the properties of the molecules and relate them to specific three dimensional configurations. In order to obtain effective devices and to identify structural modifications which could affect the required characteristics, comprehensive knowledge of the treated materials and their related compounds is fundamental. This could be achieved by developing efficient strategies which combine existing synthetic technologies and experimental fabrication methods, with both simple and sophisticated computational methodologies to explore at the molecular, atomic and electronic levels the characteristic features of the supramolecular aggregates. Integrated approaches involving different combinations of computational schemes have been used successfully to investigate the spectroscopic properties of various probes in numerous environments,²²⁻²⁹ but few^{30,31} of them has focused their attention on the spectroscopic properties of dyes grafted onto amorphous polymeric materials.

In the present work an effective computational strategy, able to simulate real-size systems over length scales of tens of nanometers for long sampling times, is defined to flank and support experiments. In order to demonstrate its efficiency, this improved multi-level approach has been applied to the study of a specific dye, namely 4-naphtoyloxy-1-methoxy-2,2,6,6-tetramethylpiperidine (NfO-TEMPO) grafted onto an apolar polymer matrix, which was investigated experimentally by Passaglia and co-workers.^{32,33} The behavior of this dye in toluene solution and its spectroscopic properties were already studied through a combination of theoretical and experimental methodologies and the results were reported and exhaustively discussed in a previous paper.³⁰ It turned out that maximum

absorption and emission wavelengths, spectral line shapes and Stokes shifts were very well reproduced by the proposed computational protocol, which was based on a time-dependent statistical description of the whole system represented by explicit molecules. The method has been now further extended, to describe a more complex environment, a polyethylene-based material, and to reproduce and interpret, beside the dynamics of the dye inside the matrix, its vibrational characteristics and absorption/emission spectra under the perturbation of external sources. Very recently,³⁴ a flavor of the general strategy employed was given, focusing the discussion on the nature of flexible cages, formed by the polymer embedding around the dye, and their effects on the emission band shapes. Here the computational approach is presented and discussed in detail, and a deep insight onto the microscopic behavior of the functionalized polymer is achieved through the computation of the most relevant structural, dynamic and spectroscopic data.

As far as the computational methods integrated in the present approach are concerned, they range from empirical force field (FF) based molecular dynamics (MD) simulations to full quantum mechanical (QM) calculations. Indeed, considering that changes in the conformation or response of polymer-grafted dyes can be due to the influence of the chemical/physical environment which they are inserted in, and that these perturbations can be markedly reflected in the fluctuations of fluorescence intensity, spectral shape and position^{35–38} and other properties,^{39–41} an explicit time-dependent approach has been employed in order to obtain a more direct comparison with experimental results. As already discussed, the FF based simulations are capable of describing the dye in a realistic environment and follow the evolution of the whole system to its most probable configurations over time scales longer than 100 ns. Calculations of spectroscopic properties are very sensitive to chromophore structure variations and thus require highly accurate and reliable force field parameters. For this reason the FF parameterization of the dye used in this work was performed with JOYCE,^{30,42,43} and consisted in specifically deriving all the intramolecular parameters, necessary to describe the chromophore in its ground (GS) and electronically excited (EES) state, from QM calculations by fitting optimized energies, gradients and Hessian matrices.

2 Computational Details

2.1 Scheme of the approach

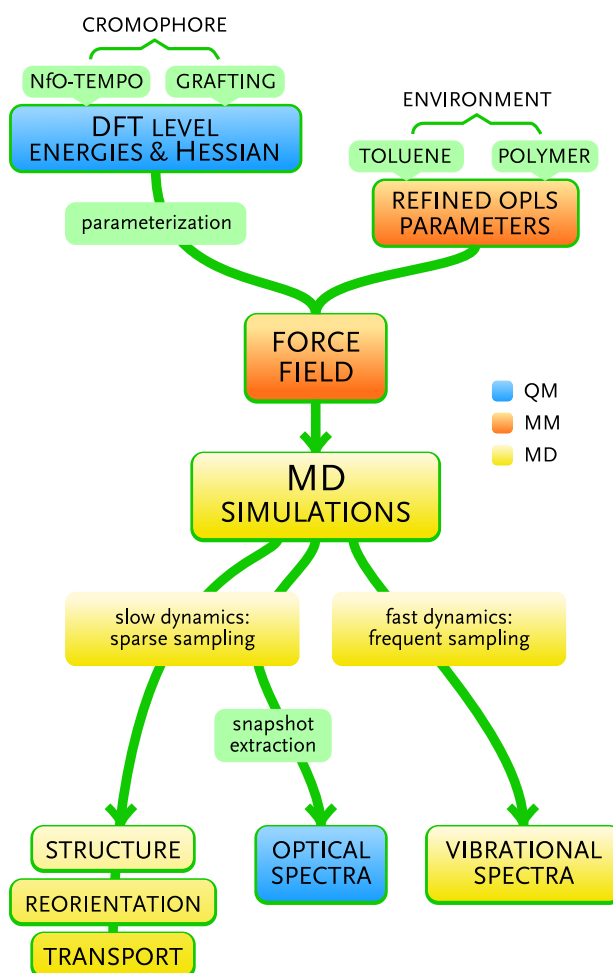


Figure 1: Flowchart describing the main steps accomplished to model the investigated dye in different environments, making use of both QM (blue) and MM/MD (orange) calculations.

The procedure, outlined in Figure 1 and adopted in the present work consists of the following steps:

1. To describe the whole chromophore + environment system, a FF is assembled by merging literature parameters for the considered embedding media and a specific description of the dye in its GS and EES, respectively. The latter was obtained

through FF parameters purposely derived from DFT and TD-DFT calculations through the JOYCE procedure.

2. MD simulations are performed with a two-fold objective: sampling reliable sets of configurations over long time scales, to describe system structure and slow dynamics, and obtaining highly correlated trajectory points to address fast dynamics.
3. The first set is employed to investigate both the structural properties and the translational and orientational features of the systems. A subset of more sparsely sampled configurations is also used to obtain resolved UV-visible spectra, resorting to QM and multilayered QM/MM computations.
4. The more correlated set is instead employed to produce the vibrational spectra of the chromophore embedded in the considered environment.

Details about FF parameterization are given in section 2.2; MD simulations and the related analysis are described in sections 2.3 and 2.4, respectively; finally, the QM and QM/MM calculations are detailed in section 2.5.

2.2 Accurate and specific FF parameterizations

The FF parameters employed in all MD simulations were specifically assembled for the NfO-TEMPO chromophore grafted onto the polymer matrix. On the contrary, as far as the functions subtending the FF expression are concerned, standard bonded and non-bonded equations were adopted, as detailed in the following.

$$E^{FF} = E_{stretch} + E_{bend} + E_{Rtors} + E_{Ftors} + E_{nb} \quad (1)$$

The first three terms refer respectively to "stiff" bonds, angles and dihedrals, being represented with harmonic potentials:

$$E_{stretch} = \frac{1}{2} \sum_{\mu}^{N_{bonds}} k_{\mu}^s (b_{\mu} - b_{\mu}^0)^2 \quad (2)$$

$$E_{bend} = \frac{1}{2} \sum_{\mu}^{N_{angles}} k_{\mu}^b (\theta_{\mu} - \theta_{\mu}^0)^2 \quad (3)$$

$$E_{Rtors} = \frac{1}{2} \sum_{\mu}^{N_{Rdihedrals}} k_{\mu}^t (\phi_{\mu} - \phi_{\mu}^0)^2 \quad (4)$$

Sums of periodic functions are instead employed to represent flexible "soft" dihedrals (Fdihedrals, δ_{μ}):

$$E_{Ftors} = \sum_{\mu}^{N_{Fdihedrals}} E_{Ftors,\mu} = \sum_{\mu}^{N_{Fdihedrals}} \sum_j^{N_{cos\mu}} k_{j\mu}^d [1 + \cos(n_j^{\mu} \delta_{\mu} - \gamma_j^{\mu})] \quad (5)$$

where $N_{cos\mu}$ is the number of cosine functions employed for the δ_{μ} dihedral. The last term of Equation (1), $E_{nbintra}$, contains the non-bonded interactions, computed as a sum of a Coulomb and Lennard-Jones (LJ) terms, *i.e.*

$$E_{nbintra} = \sum_i \sum_{i<j} c_{ij} \frac{q_i q_j}{r_{ij}} + \sum_i \sum_{i<j} 4\epsilon_{ij}^{intra} \left[\left(\frac{\sigma_{ij}^{intra}}{r_{ij}} \right)^{12} - \left(\frac{\sigma_{ij}^{intra}}{r_{ij}} \right)^6 \right] \quad (6)$$

As indicated in the previous section, in order to model the dye grafted onto the polymeric matrix, three regions have been identified and described with different FF parameter sets, to be used in Equation (1). Each portion, sketched in Figure 2, was thus parameterized as follows.

- i) The polymer matrix was constructed by randomly branching a single linear aliphatic hydrocarbon chain composed by more than 1400 Carbon atoms, described at full atomic level. Each branching was achieved by replacing a methylene H atom with an ethylene moiety every 9, 10 or 11 CH₂ monomer units of the principal chains, thus obtaining a model polymeric branched chain described by 4655 atoms. The FF for the model polymer was first built by transferring literature parameters^{44,45} for aliphatic hydrocarbons. Preliminary MD runs at atmospheric pressure and temperature at 300 K were performed to equilibrate the system, whose final density was slightly less than 850 kg/m³, which is slightly lower than the average experimental range (860-940 kg/m³) reported^{46,47} for low density PE polymers. As a matter of fact, this density issue for long aliphatic chains has recently been observed⁴⁸ and corrected by a refinement procedure. Here, to circumvent this problem, an alternative approach⁴⁹ has been adopted, where all Carbon's and Hydrogen σ 's in Equation (6) were reduced by 5%, achieving a final value of 890 kg/m³, after an equilibration time of ~ 5 ns.

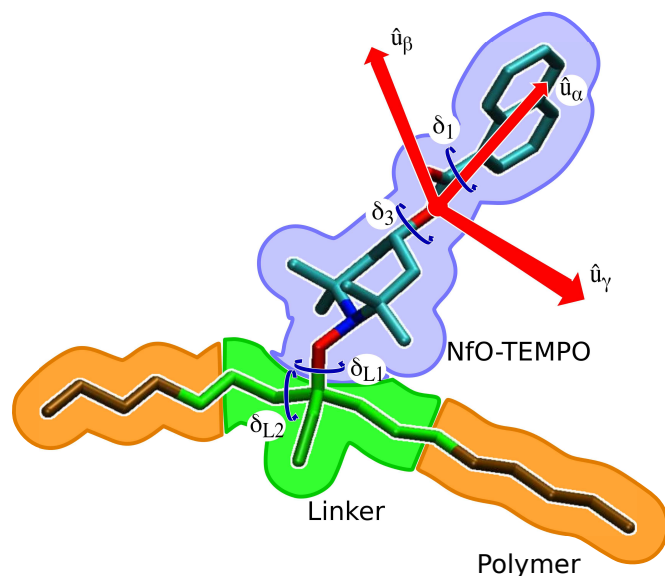


Figure 2: Modeling of the dye-polymer junction. The three regions identified within the chromophore + environment system are indicated with different colors: cyan, red and blue for the NfO-TEMPO dye, green for the grafting junction and brown for the polymer. The Hydrogen atoms and the main part of the polymer chain are not displayed for clarity. The three main inertia axes are also shown (red arrows) together with the most flexible dihedrals (δ_1 , δ_3 , δ_{L1} , δ_{L2}), indicated by bent arrows.

- ii) The FF parameters for the dye's GS and EES were taken from an earlier work,³⁰ where a specific intramolecular parameterization, based on QM data computed at DFT and TD-DFT level, was performed on the NfO-TEMPO dye with the JOYCE procedure^{42,43} to reproduce structural and spectroscopic properties of the dye in toluene solution.
- iii) The grafting process³³ was mimicked by linking the TEMPO Oxygen atom to a branched site of the polyethylene chain, after removal of the corresponding H atom. An hybrid strategy was adopted to define FF parameters in the grafting region: non-bonded parameters were taken from the literature,⁴⁴ stretching and bending parameters were transferred from the NfO-TEMPO GS FF³⁰ and parameters concerning the dihedrals located in the dye-polymer junction were specifically parameterized through Equation (5) and a least square minimization procedure, on purposely computed QM torsional energy scans, performed on small model molecules as shown in Figure 3.

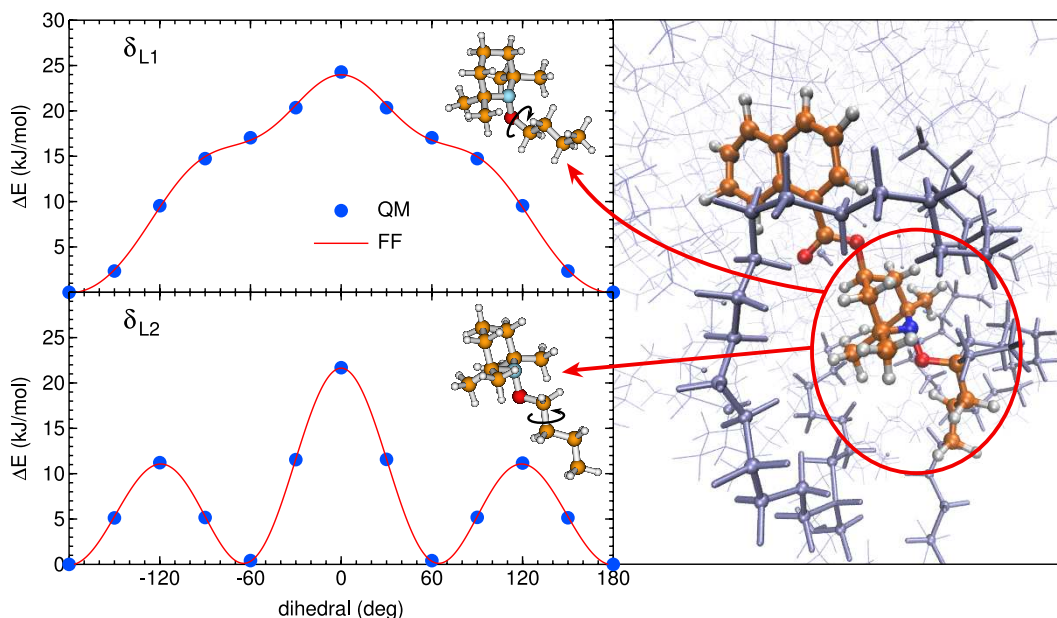


Figure 3: Left panel: specific parameterization of the torsional profiles in the grafting TEMPO-polymer region. The small molecular targets employed as models for the grafting region are shown in the insets. QM data, computed at the PBE/N07D level, are reported with blue circles, while the parameterized FF torsional profile is shown with a red solid line. Right panel: TEMPO-polymer grafting region and selection of the small molecular targets.

To avoid highly repulsive interactions, the NfO-TEMPO dye was linked onto a non equilibrated strained conformation of the polymer, where most of the aliphatic chain dihedrals were in their *trans* configuration. Thereafter, an effective entangling of the chain was achieved with short equilibration runs in the NVT ensemble, where the NfO-Tempo dye was frozen at its equilibrium conformation. During these runs, the volume of the simulation box was slowly decreased and the torsional barriers of the chain dihedrals were artificially lowered to increase the rate of conversion from the *gauche* to the *trans* conformation. After 10 ns, a pressure coupling was introduced and all the constraints on the dye substituent were removed. The final NPT simulation run 10 ns long was performed at 300 K and 1 atm, achieving again the final density of 890 kg/m³. It may be worth mentioning that the experimental concentration of the dye inside the polymer is so low that the grafted molecule cannot be found in close proximity to another probe, hence the choice of modeling just one molecule per polymer chain should best represent this scenario.

2.3 MD Simulations

MD simulations were performed on four different systems, namely the isolated dye, NfO-TEMPO in toluene solution, linear low density polyethylene (LLDPE) bulk phase and one NfO-TEMPO chromophore grafted onto the LLDPE bundle. All MD simulations were carried out with GROMACS4.5⁵⁰ using of the afore described FFs.

In all simulations, except those carried out for the isolated dye, periodic boundary conditions were applied in all directions and the simulation time step was set to 0.5 fs, unless otherwise stated. Long-range electrostatic interactions were treated with the particle mesh Ewald (PME) method, whereas a 13 Å cutoff was applied to the van der Waals interactions. All condensed phase systems were first equilibrated in the NPT ensemble, coupling the system to a thermal bath at $T = 300$ K (with a coupling constant of 0.1 ps) and a pressure bath with $P = 1$ atm (with a coupling constant of 1.0 ps) through the Berendsen's coupling scheme.⁵¹ Starting from the equilibrated structures, NPT production dynamics were carried out storing the trajectories every 0.5 ps for further analysis of structural and thermodynamic properties. As far as the dye is concerned, GS and EES FFs³⁰ were employed for all the NPT production runs. As regards the simulation of the isolated dye, equilibration and production runs were performed in the NVT ensemble, without periodic boundary conditions and the same temperature coupling scheme (300 K).

The final structures obtained in all NPT simulations involving NfO-TEMPO (*i.e.* in the gas phase, in toluene and grafted to the polymer matrix) in its GS conformation were further equilibrated for 1 ns in the NVT ensemble, and thereafter simulated in the micro-canonical NVE ensemble to investigate dynamical properties of the systems. In view of the fast processes to be investigated, the NVE time step was decreased to 0.2 fs and the trajectories stored every 5 fs (*i.e.* 25 steps) and 0.4 fs (2 steps) for transport and vibrational properties, respectively. The total NVE simulation time was 5 ns in the former case, 1 ns in the latter.

2.4 Trajectory analysis

The structural properties of the grafted NfO-TEMPO were studied by means of the pair correlation function $g(r)$, computed between the dye center of mass and the methylene units of the polymer chain. To get a deeper insight on the effect of the polymer on the dye's properties, comparisons were also made with the results obtained from previous³⁰ MD runs, both *in vacuo* and in toluene solution. It is worth noticing that, for a more straightforward comparison with the results obtained for the functionalized polymer, in the case of toluene solution $g(r)$ was here re-computed as a function of the distance between NfO-TEMPO center of mass and toluene's aromatic C atoms (instead of toluene's center of mass³⁰). Furthermore, the conformational properties of the internal structure of the dye have been studied by investigating the dihedral distributions averaged over the MD trajectories.

For a more precise characterization of the local interactions between the dye and its different embeddings, the first fragment coordination shell (whose radius can be identified from the first minimum in the $g(r)$ function) was also described in terms of residence times. Residence times are calculated from the time auto correlation function (ACF):

$$R(t) = \langle \Theta_n(t_0) \Theta_n(t_0 + t) \rangle \quad (7)$$

where the Heaviside function $\Theta_n(t)$ is 1 if the n -th unit (methylene moiety or toluene molecule, for polymer or simple solvent, respectively) is inside the first solvation shell at time t , and 0 otherwise. The $\langle \dots \rangle$ symbol indicates a double average over the time origins t_0 and the N_{shell} units within the shell at each t_0 . $R(t)$ can be interpreted as the probability that a neighboring unit remains within the first shell after a time t . As far as the polymer is concerned, the methylene groups directly connected with the linking region are excluded, as they cannot exit the solvation region.

Translation and rotation of the dye have been studied both in toluene solution and inside the polymer matrix. The isotropic translational diffusion coefficient is defined as

$$D = \lim_{t \rightarrow \infty} D(t) = \lim_{t \rightarrow \infty} \frac{1}{6t} \langle [\mathbf{r}(t_0) - \mathbf{r}(t_0 + t)]^2 \rangle \quad (8)$$

where $\langle \dots \rangle$ indicates the average over all time origins. Molecular spinning and tumbling

are described by the rotational diffusion coefficients D_k^R :

$$D_k^R = \int_0^\infty \langle \omega_k(t_0) \cdot \omega_k(t_0 + t) \rangle dt \quad ; \quad k = \hat{u}_\alpha, \hat{u}_\beta, \hat{u}_\gamma \quad (9)$$

where \hat{u}_α , \hat{u}_β and \hat{u}_γ are the three main inertia axes of the dye, indicated in Figure 2 and $\omega_k(t)$ is the angular velocity at time t around axis \hat{u}_k . Complementary information about dye spinning and tumbling are also retrieved by calculating the reorientation of the abovementioned axes. Indeed, re-orientational times are expressed as

$$\tau_k^l = \int_0^\infty \langle P_k^l(t) \rangle dt \quad ; \quad k = \hat{u}_\alpha, \hat{u}_\beta, \hat{u}_\gamma \quad (10)$$

where $P_k^1(t)$ and $P_k^2(t)$ are the first and second rank Legendre polynomial of the function $\cos[\phi_k(t)]$, $\phi_k(t)$ being the angle between $\hat{u}_k(t)$ and $\hat{u}_k(0)$. The functions $\langle P_k^l(t) \rangle$ from the MD trajectories are fitted by a sum of exponentials

$$\langle P_k^l(t) \rangle \sim \sum_{i=1}^{Nexp} c_i^{k,l} e^{-(t/\tau_i^{k,l})} \quad (11)$$

whose time integrals can be determined analytically.

IR absorption cross-section for a quantum molecular system at thermal equilibrium at a given frequency ω is⁵²

$$\alpha(\omega) = \frac{4\pi^2\omega}{3\hbar c} (1 - e^{-\frac{\hbar\omega}{k_B T}}) I(\omega) \quad (12)$$

where k_B is the Boltzmann constant, T the temperature and the last factor $I(\omega)$ represents the ‘‘line-shape function’’

$$I(\omega) = \frac{1}{2\pi} \int_0^\infty e^{i\omega t} \langle \hat{\mathbf{M}}(t_0) \cdot \hat{\mathbf{M}}(t_0 + t) \rangle dt \quad (13)$$

which is expressed in terms of the dipole moment operator $\hat{\mathbf{M}}$. In the computational picture employed here, only classical quantities are available from the MD simulations, thus requiring to substitute the dipole operator with its counterpart

$$\hat{\mathbf{M}} \rightarrow \mathbf{M}_{cl} \equiv \sum_{i \in \text{mol}} q_i \mathbf{r}_i \quad (14)$$

and to calculate the ACF over discrete trajectories subjected to classical statistics, thus exploiting the classical line-shape

$$I_{cl} = \frac{1}{2\pi} \int_0^\infty e^{i\omega t} \langle \mathbf{M}_{cl}(t_0) \cdot \mathbf{M}_{cl}(t_0 + t) \rangle dt \quad (15)$$

where the average is taken over the time origins t_0 . It has been pointed out⁵³ that this formulation of the line-shape does not respect the “detailed balance” condition for non-zero temperatures.⁵⁴ Therefore, a quantum correction function must be used, in order to approximate better the exact $I(\omega)$ as $Q_{QC}(\omega, T)I_{cl}$. Among the several available models,⁵⁵ the so-called “harmonic” approximation is used here

$$Q_{QC}(\omega; T) = \frac{\frac{\hbar\omega}{k_B T}}{1 - e^{-\frac{\hbar\omega}{k_B T}}} \quad (16)$$

In brief, the vibrational spectra were calculated as

$$\alpha(\omega) = \frac{2\pi\omega^2}{3ck_B T} \int_0^\infty e^{i\omega t} dt \langle \mathbf{M}_{cl}(t_0) \cdot \mathbf{M}_{cl}(t_0 + t) \rangle \quad (17)$$

UV-visible spectra were derived by averaging QM calculations performed over different sets of snapshots, purposely extracted from the trajectory as indicated in the following.

- i) A set of frames was extracted from the simulation *in vacuo*.
- ii) Two further sets were instead created by sampling the trajectory of the MD simulation of the dye grafted onto the polymer. The first of these sets was extracted according to a mechanical embedding (ME) scheme, where only the dye geometrical variations, induced by the presence of surrounding polymeric matrix, are retained. To this end, the NfO-TEMPO coordinates are extracted from each MD snapshot together with the C atom bearing the dye-polymer linkage, and the latter site is saturated with three H atoms.
- iii) The direct electrostatic interaction between the dye and the surrounding matrix can be accounted more explicitly within the electrostatic embedding (EE) scheme, by placing in the snapshots both the grafted dye and a relevant region (*vide infra*) of its surroundings.

Further details of the procedure can be found in an earlier work.³⁰

2.5 QM calculations

Torsional energy scans, needed for the linkage FF parameterization, were performed at the same level of theory (PBE0 DFT functional with the N07D basis set⁵⁶) employed in

the NfO-TEMPO parameterization, reported in a previous work.³⁰ During the scan, the absolute energy minimum was obtained by a complete geometry optimization, whereas the other geometries were identified by optimizing the energy without any restriction except the investigated dihedral angle, which was increased in a stepwise manner.

Similarly, following the protocol proposed and validated in Ref.,³⁰ all electronic transitions employed in Equation (18) were computed by means of the TD-DFT method, using the CAM-B3LYP functional coupled with the cc-pvDZ basis set. In both ME and EE schemes the saturated dye is considered explicitly, but in the latter the surrounding polymer atoms were also taken into account by replacing them with point charges. The vertical transition energies were computed on each snapshot and convoluted with Gaussian functions in the energy domain with half width at half maximum (Δ_ν) of 0.05 eV. Thus, the resulting spectrum computed for the c -th frame is

$$\epsilon_c(\nu) \propto \sum_{i \in \text{states}_c} \frac{f_{c,i}}{\Delta_\nu} \exp \left[\left(\frac{\nu - \nu_{c,i}^0}{\sigma_\nu} \right)^2 \right] \quad (18)$$

where

$$\sigma_\nu = [2\sqrt{2\ln(2)}]^{-1} \cdot \Delta_\nu$$

and $\nu_{c,i}^0$ and $f_{c,i}$ are the frequency and the oscillator strength of the i -th excitation, respectively. For a direct comparison with the experimental data, the energy spectrum is then plotted in the wavelength domain ($\epsilon_c(\lambda)$). The signals originating from each snapshot are then averaged according to the equation:

$$\bar{\epsilon}(\lambda) = \sum_{c \in \text{snap}} \frac{\epsilon_c(\lambda)}{N_{\text{snaps}}} \quad (19)$$

to achieve the final "statistical" UV-VIS spectrum.

All QM calculations were performed with the Gaussian software.⁵⁷

3 Results and Discussion

3.1 Structural properties

The four investigated systems, consisting of the dye in its GS or EES, embedded in in toluene (**T**) and polymer (**P**), were labeled as **GS@T**, **EES@T**, **GS@P** and **EES@P**.

For each system, NPT simulations were carried out at constant temperature (300 K) and pressure (1 atm) for 10 and 20 ns. MD trajectories were stored every 0.5 ps, and firstly used to compute the pair correlation functions (reported in Figure 4) between the dye center of mass and the surrounding heavy atoms (*i.e.* aromatic and methylene Carbons for toluene and polymer environments, respectively). Despite all functions present a

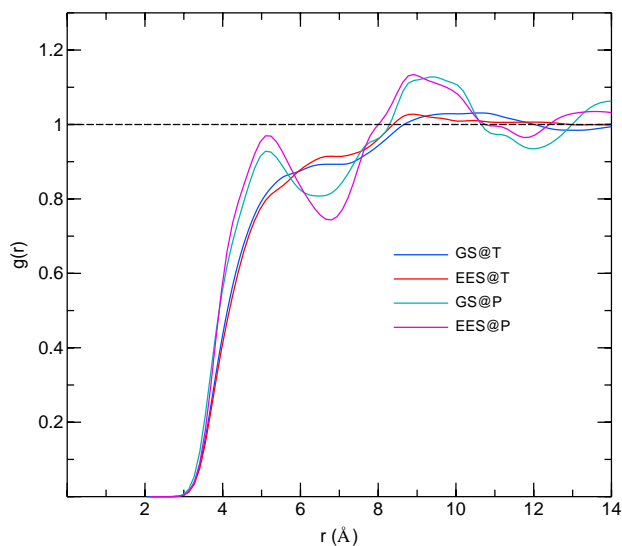


Figure 4: Pair correlation functions between the NfO-TEMPO center of mass and the surrounding aromatic (toluene, blue and red lines for GS and EES, respectively) or aliphatic (polymer, turquoise and magenta) carbons.

similar starting behavior, the influence of the surroundings rapidly differentiates their shapes, with the $g(r)$'s computed in polymer much more structured than those computed in solution. On the other hand, the correlation functions of different electronic states (GS and EES) embedded in the same *medium* are less distinguishable. Comparison of the first peaks in toluene and polymer ($\sim 5.8 \text{ \AA}$ and 4.8 \AA , respectively) shows that, for both GS and EES, the polymer units are allowed to get sensibly closer to the dye, suggesting that a tighter cage is formed around the naphthalene moiety by the entangled polymer. The well defined minimum of the first peak in polymer and the absence of a net decay in toluene suggest a longer lifetime of the polymer cage and a more "dynamic" character of the toluene first neighbor shell. Moving to longer distances, the second peak is centered at similar values ($\sim 9 \text{ \AA}$) for all the investigated systems, but the structure of the toluene

embedding is almost completely lost.

A deeper insight on the surrounding environment and its correlation with the molecular

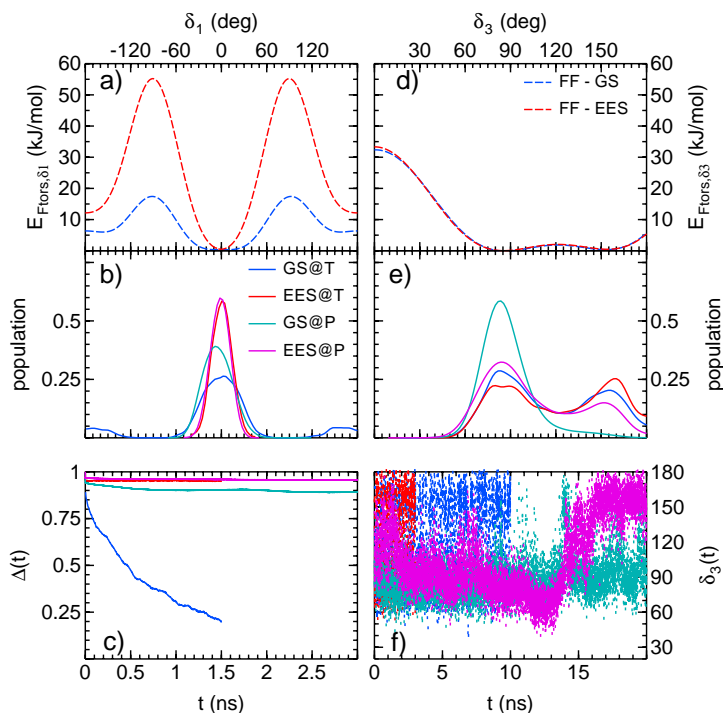


Figure 5: Torsional profiles (kJ/mol), population distributions (a.u., normalized peak area), normalized dihedral time correlation function $\Delta(t)$ and instant values of δ_1 and δ_3 (see Figure 3) of the NfO-TEMPO dye in **GS@T**, **EES@T**, **GS@P** and **EES@P** systems (blue, red, turquoise and magenta, respectively). a) δ_1 torsional profile ; b) δ_1 MD distribution ; c) δ_1 time correlation ; d) δ_3 torsional profile ; e) δ_3 MD distribution ; f) δ_3 over time.

conformations adopted by the dye can be gained by investigating the behavior of the NfO-TEMPO δ_1 and δ_3 dihedral angles (see Figure 3), which were found to remarkably influence^{30,58} both the dye's shape and its optical response. In the two middle panels of Figure 5 the distributions of the dihedral angles in the dye's GS and EES are shown for both environments. To aid the discussion, the FF torsional potentials (*i.e.* $E_{Ftors,\mu}$ entering in equation (5), with $\mu=\delta_1, \delta_2$) subtending each considered dihedral rotation and parameterized in Ref. [30] are reported in the top panels. As already noted in that previous work, as could be expected from the inspection of the torsional profiles, δ_1 distribution in toluene is significantly narrower for the EES, and its maximum is centered at about 0° , which corresponds to one of the possible planar conformations. Since this reduced

flexibility has been ascribed³⁰ to the increased delocalization of the π cloud towards the regions in proximity of the TEMPO moiety (which is an intrinsic feature of the dye) it is not surprising that the same behavior is found when the dye in its EES is embedded in a different environment like PE. On the contrary, a major difference, rooted in the different embedding, is evident when comparing the GS δ_1 distributions obtained for the **GS@T** and **GS@P** systems. In fact, only in the former solvent the dye is able, as already found in previous work,³⁰ to adopt the two planar conformations ($\delta_1 \sim 0^\circ$ and $\delta_1 \sim \pm 180^\circ$) expected from the inspection of the corresponding torsional energy profile (see left-top panel of Figure 5), whereas only the $\delta_1 \sim 0^\circ$ conformer is populated in the polymer matrix. This observation is in agreement with the hypothesis drawn from the $g(r)$ analysis, where the polymeric chain entangles the dye, thus reducing its internal flexibility. This is also confirmed by looking at the δ_1 time ACF

$$\Delta(t) = \langle \cos[\delta_1(t_0 + t)] \cos[\delta_1(t_0)] \rangle$$

registered for all systems and displayed in panel c) of Figure 5. Indeed, only in toluene solution the dye in its GS is free to explore all the accessible conformations, being $\Delta(t)$ almost zero after 1.5 ns. On the contrary, the ACF in **GS@P** remains highly correlated for more than 3 ns, indicating that the carboxy moiety is forced by the embedding *medium* to preserve its coplanarity with the naphthalene unit.

Analogous data computed for δ_3 and shown in the left panels of Figure 5 are apparently in contrast with the above analysis. Indeed, the described "caging" effect of the polymer is only evident in the GS, whereas the dye in its EES seems able adopt conformations similar to those observed in toluene solution. However, the similar behavior of the δ_3 distributions in **EES@T** and **EES@P** can still find a rationale without contradicting the "caging" hypothesis. Indeed, if the value of δ_3 is plotted over the simulation time (see bottom right panel) a remarkable difference appears: in toluene fast inter-conversions between the two conformers are allowed, whereas in the more hindered polymer matrix only one very slow (~ 12.5 – 17 ns) transition is found from one conformer to the other, whereas only small variations of the dihedral angle are allowed by the cage for shorter time scales.

The "caging" role of the polymeric matrix can be further investigated by closer in-

spection of the mean interactions between the dye and its embedding *medium* and by the analysis of the dynamic features that characterize the first neighbor shells. The mean field due to the surroundings and experienced by a dihedral δ_μ of the embedded dye can be derived from the knowledge of the computed dihedral distribution function $P(\delta_\mu)$ and the FF term $E_{Ftors,\mu}$ given by Equation (5). In the hypothesis that the effective potential energy curve governing δ_μ dynamics can be partitioned into an intra molecular component (*i.e.* $E_{Ftors,\mu}$) and the mean field $W(\delta_\mu)$, $P(\delta_\mu)$ can be expressed as

$$P(\delta_\mu) \propto e^{-\frac{E_{Ftors,\mu} + W(\delta_\mu)}{k_B T}} \quad (20)$$

and therefore, up to an additive constant,

$$W(\delta_\mu) = -(E_{Ftors,\mu} + k_B T \ln[P(\delta_\mu)]) \quad (21)$$

The above equations are applied to δ_1 , and the resulting mean field $W(\delta_1)$ is displayed in the right panel of Figure 6, together with all the quantities employed for its derivation (left panel). By looking at the left panel, it is evident how the presence of the polymer

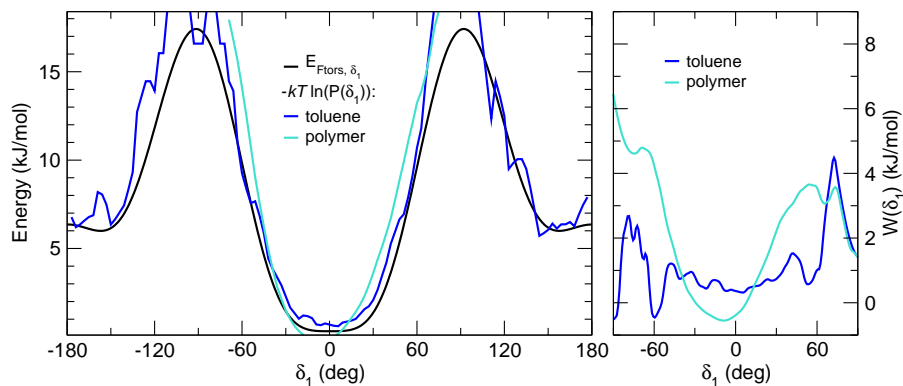


Figure 6: Left: Comparison between the intra-molecular contribution (E_{Ftors,δ_1} , black line) and the total field experienced by the dye in toluene (blue line) and polymer matrix (turquoise line). Right: Mean field $W(\delta_1)$ due to the environment.

cage remarkably alters the effective torsional potential that the dye experiences on its δ_1 dihedral. In fact, differently from the simulation in toluene solution, where the torsional profile remains essentially unchanged with respect to the original FF term, the simulation of the dye inside the polymer does not present local minima in the regions around

$\pm 180^\circ$ which are no more accessible, due to the presence of the cage, whose "walls" constrain the dihedral to librate within the $[-60^\circ, 60^\circ]$ interval. The same scenario is shown by the mean fields reported in the right panel, where the marked difference between the two surrounding *media* is even more evident, $W(\delta_1)$ in toluene being much flatter and close to 0, thus almost not perturbing the dye flexibility and average shape. It is also worth noticing that the entanglement of the polymer around the dye creates a supplementary well, centered at $\delta_1 \sim 0^\circ$, that constrains δ_1 to librate within a limited range rather than rotate almost completely, as could be instead expected from its internal torsional potential.

Further characterization of the caging environment that takes place within the polymer embedding can be gained by looking at the residence ACF, defined in Equation (7), computed for the NfO-TEMPO GS in both *media* and reported in Figure 7. After a few

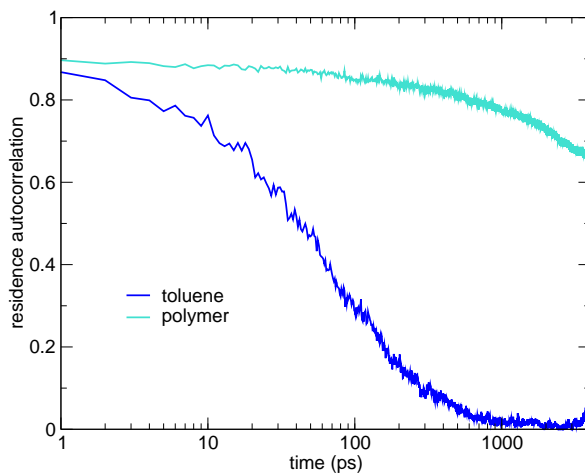


Figure 7: Residence ACF computed, according to Equation (7), over the dye's first neighbor shell in toluene (blue line) and polymer (turquoise) surroundings.

ps the faster ACF decay in toluene becomes evident (0.5 after ~ 30 ps). This means that, after this time, around half of the toluene molecules forming the first neighbor shell (at time t_0) have abandoned the sphere, exchanging place with second neighbor molecules. This process leads to a complete renewal of the original first neighbor shell in less than 1 ns. On the contrary the residence ACF in polymer never vanishes in the first 3 ns observed, its final computed value being ~ 0.6 . Furthermore, the ACF is rather flat

(around 0.9) for 200 ps, testifying a remarkably slow motion of the polymer methylene units surrounding the dye, thus in agreement with the scenario of a well defined cage hindering the conformational flexibility of the grafted chromophore.

3.2 Dynamic properties

A deeper insight into the effect of the different embeddings on the dye's dynamics can be gained by comparing the NfO-TEMPO translational and rotational dynamic properties, computed in the two cases. Since only a negligible dependence over the electronic state of the dye was found in the previous analysis of the structural features in the two embeddings, NVE simulations and the consequent analysis of both translational and rotational dynamics were limited to the GS.

As far as translational diffusion is concerned, the mean square displacement (MSD) of the dye's center of mass was computed for **GS@T** and **GS@P** systems and showed in Figure 8. As expected, striking differences appear in the diffusion exhibited by the dye in the different embeddings. In fact, while the dye in the **GS@T** system reaches, after

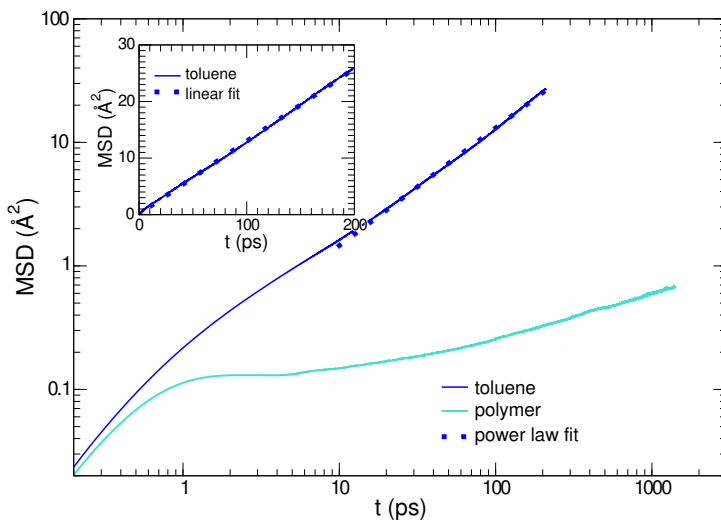


Figure 8: Big panel: comparison in logarithmic scale between $\text{MSD}(t)$ of the dye in the two different environments: toluene solution and grafted to polymer. Inset: The MSD curve for the system in solution is shown in linear scale. Analytic fits of the curve in the $t > 80$ ps region are reported.

few ps, the diffusive regime characteristic of a molecular solute in a simple liquid solvent, a well visible plateau appears instead in the matrix, switching to a linear behavior after

~ 100 ps. More specifically, when the dye is solvated in toluene, the $MSD(t)$ can be fitted linearly, and from the slope of the resulting line a translational diffusion coefficient $D_{\text{tol}}^{\text{tr}} = (0.66 \pm 0.04) \cdot 10^{-9} \text{m}^2 \text{s}^{-1}$ is obtained. On the contrary, the MSD features of the dye grafted onto the polymer matrix closely recall a sub-diffusive behavior, already reported for several systems, among which ionic liquids,⁵⁹ disordered crystals,^{60–62} super-cooled liquid crystals^{63,64} and polymers.^{65–67} In all these cases, the sub-diffusive features were connected to the presence of a long-lived cage, that surrounds the target solute and delays the incoming of the diffusive regime. In the **GS@P** system, the plateau exhibited by the MSD can also be interpreted as the signature of a β -relaxation (sub-diffusive) regime, that takes place from the end of the pure ballistic dynamics (hundreds of femtoseconds) to the onset of the linear behavior, which occurs after ~ 100 ps. Indeed, when the solute is trapped (β regime), its displacement is restricted, and a plateau appears in the MSD . It should be pointed out that the sub-diffusive regime observed through the RMSD of the solute indicates the polymer units, covalently bonded to it, are slowly diffusing too, and that the polymer itself is not glassy. The sub-diffusive behavior observed in the dye can thus be explained in two ways: on the one hand, the intrinsic sub-diffusive character of the polymer matrix dynamics is transmitted to the dye through the grafting linkage, on the other hand, the "polymer cage" characterized by the previous analysis, prevents the dye from reaching a true diffusive regime.

A further characterization of the cage can be obtained by the analysis of the dye rotational behavior. Indeed, it can be expected that the polymer entanglement not only decreases the dye's conformational flexibility, as previously discussed, but also limits the rotational dynamics and, therefore, the possible orientations of the dye with respect to the embedding. The angular velocity ACF was obtained for the two embeddings with respect to the three inertia axes (\hat{u}_α , \hat{u}_β and \hat{u}_γ) sketched in Figure 2. More specifically, rotation around axis \hat{u}_α can be considered as a spinning motion, whereas rotation around \hat{u}_β and \hat{u}_γ drive the tumbling. The resulting ACF, shown in the upper panel of Figure 9 was integrated according to Equation (9) to obtain the rotational diffusion coefficients, reported in Table 1. Two main conclusions can be drawn from the analysis of these data. In the first place the rotation of the tethered dye is hindered in all directions by

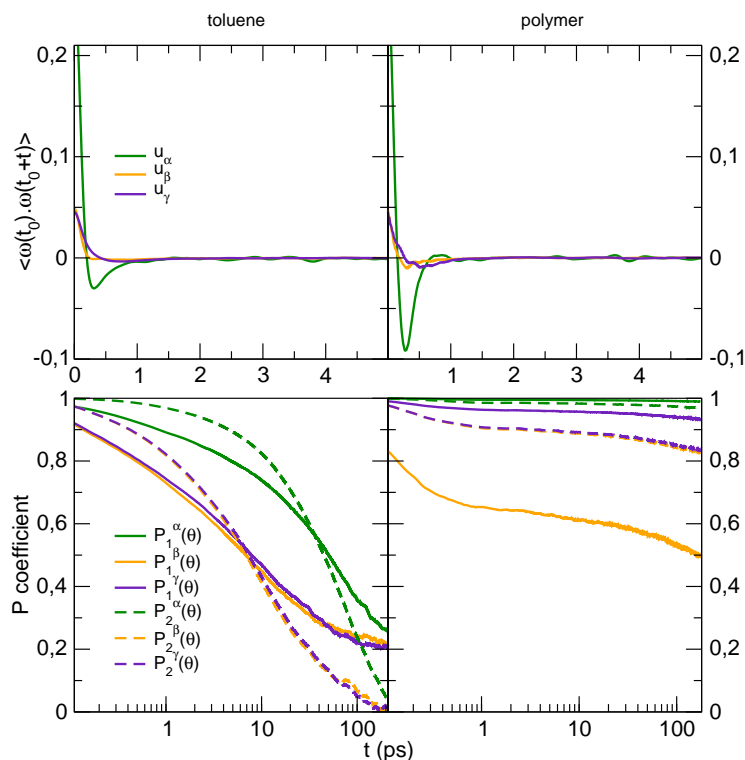


Figure 9: Rotational behavior of the NfO-TEMPO dye in the toluene (left) and polymer (right) embeddings. Top: angular velocity autocorrelation function along the three principal inertia axes; bottom: orientational first and second order parameters $P_1(\theta)$ (solid lines) and $P_2(\theta)$ (dashed lines) concerning the three axes.

the surrounding cage, with the values of the two largest rotational coefficients in toluene solution almost twice those computed in polymer. Second, the rotational dynamics of the dye is rather anisotropic in both *media*, being the spinning motion always faster than the tumbling around the other two.

A final confirmation of the quenching effect on the dye dynamics due to the embedding polymer cage comes from the comparison of the orientational relaxation behavior of the three inertia axes in the two *media*. By looking at the bottom panels of Figure 9, where the first and second Legendre polynomials of the ACF of the inertia axes are reported, it is evident that only in toluene the dye is able to deeply explore its rotational phase space, leading to a nearly vanishing long time limit of all the P_2 functions. Conversely, due to constraints imposed by the long-live polymer cage, none of the inertia axes completely loses correlation in the first 200 ps, since the relaxation times for the P_1 and P_2 coefficients

are found in the nanosecond timescale, which is in line with the time life of the cage that can be evinced from the time extension of the *plateau* exhibited by both translational diffusion and residence life-times.

3.3 Spectroscopic properties

3.3.1 IR spectra

Preliminary information regarding molecular vibrations can be obtained by performing spectral analysis of the velocity ACF of a single atom of the molecule. Because of its central position, the carbonyl oxygen was chosen as a probe and the vibrational power spectrum was calculated in this way for the simulations *in vacuo*, in solution and in polymer matrix.

The results are plotted in Figure 10. The spectra have a complex trend in the 400 – 1900 cm^{-1} region, and four peaks stand out, at around 490, 700, 800 and 1800 cm^{-1} . The third and fourth peaks are compatible with the IR ones reported in Ref.³³ as NfO-TEMPO markers, and involve normal modes essentially located on the naphthoyloxy moiety: the line at 1800 cm^{-1} is related to the carbonyl stretching, that strongly affects the velocity of the chosen Oxygen atom probe, as can be seen from the remarkable peak intensity in the power spectrum. The second line, related to the out-of-plane bending of the naphthalene hydrogen atoms, can be seen as well, since the carbonyl Oxygen is spatially close to the involved atoms. Conversely, the first two peaks are not evident in the IR spectrum, since

Property	Toluene	Polymer
D_{α}^{rot}	1.3 ± 0.4	0.07 ± 0.01
D_{β}^{rot}	0.05 ± 0.03	0.02 ± 0.01
D_{γ}^{rot}	0.02 ± 0.01	0.02 ± 0.01
τ_{α}^1	1.9 ± 0.1	31 ± 13
τ_{β}^1	59 ± 24	0.68 ± 0.33
τ_{γ}^1	19 ± 3	5.3 ± 4.3
τ_{α}^2	1.00 ± 0.02	10 ± 4.3
τ_{β}^2	1.8 ± 0.1	1.9 ± 1.7
τ_{γ}^2	1.6 ± 0.1	2.0 ± 1.4

Table 1: Transport (D_k^{rot} , 10^{10} s^{-1}) and re-orientational relaxation times (τ_k^i) in toluene (ps) and polymer (ns) environments.

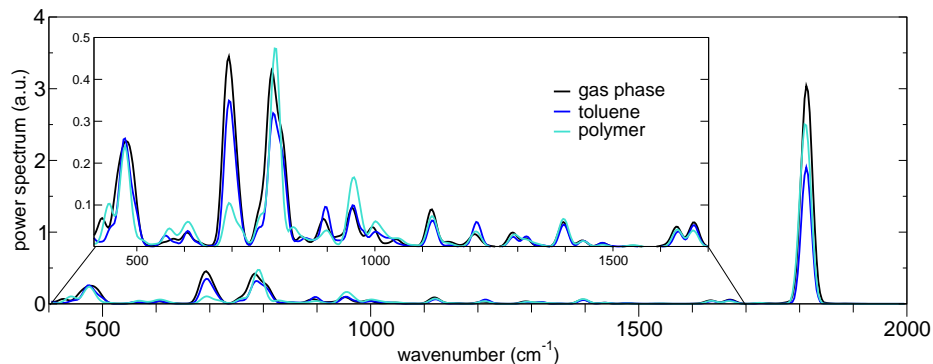


Figure 10: Power spectrum arising from the velocity autocorrelation function of the carbonyl oxygen of the NfO-TEMPO dye, for simulations *in vacuo*, in toluene and in polymer matrix. The 400 – 1700 cm^{-1} region is enlarged for clarity.

they probably correspond to IR-inactive normal modes. Moreover, from the significant suppression of the 700 cm^{-1} line when considering the grafted system, it could be speculated to assign it to an inactive normal mode located either next to the dye-polymer junction or close to the naphthalene moiety, whose large amplitude vibrations are hindered by the embedding polymer cage. Besides this latter peak, there is no further notable embedding effect. This can be explained by considering that both the solvent and the polymer are apolar and don't exhibit any specific interaction with the dye, therefore, while the large amplitude motions as dihedral rotation are actually affected by a mechanical cage effect, no substantial differences occur at shorter time scales.

In order to allow a direct comparison with experiments, the IR absorption spectrum was calculated for the isolated and the grafted dye, by using the quantum corrected Fourier transform of the electric dipole ACF, according to Equation (17). The Fourier Transform IR spectra reported in Ref.³³ for both polymer+dye and polymer alone, were used as experimental references. Since only the NfO-TEMPO atomic coordinates are included in the calculations, the dye's signal was extracted from the experimental data by taking the difference of the grafted and the isolated polymer spectrum (see Figure 11, dashed and solid turquoise lines). In the investigated window (400 - 1900 cm^{-1}), the experimental spectrum presents a faint peak around 510 cm^{-1} , followed by several peaks

delimited by the already mentioned strong ones near 800 and 1800 cm^{-1} , respectively. It can be observed that the measured vibrational modes fall within the active intervals in the power spectrum of Figure 10. Actually, modes with higher frequencies are present, though not plotted, in the experimental spectrum, with a peak reported at 3052 cm^{-1} . On the contrary these modes, related to the C–H stretching, are totally absent in the velocity power-spectrum calculated at the Oxygen site, since they do not affect this particular atom.

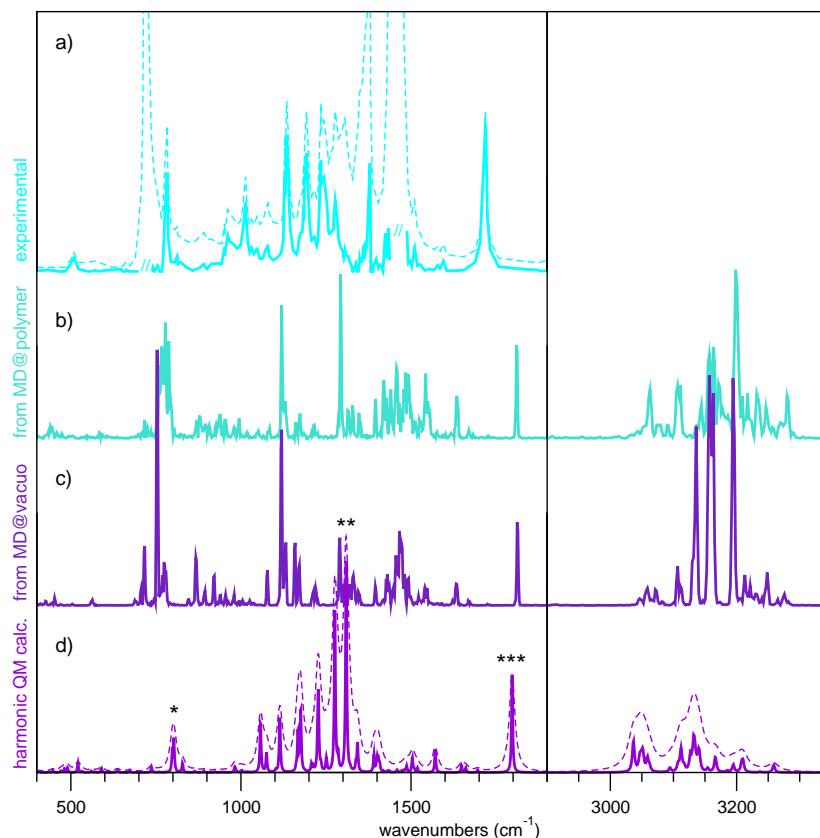


Figure 11: Experimental and computed IR spectra; from top to bottom: a) Experimental IR spectrum of the dye+polymer system (dashed line),³³ and the same spectrum removing the signals from the polymer itself (solid line). b) Calculated IR spectrum the dye, obtained from MD simulations of the grafted system. c) Calculated spectrum from MD for the NfO-TEMPO-Me *in vacuo*. d) Harmonic IR spectrum calculated at the DFT level on the isolated molecule, broadened with Lorentzian functions with HWHM 2 cm^{-1} (solid line) and 10 cm^{-1} (dashed line).

To make the crude assignment of the IR absorption lines more accurate, also the harmonic DFT-level calculation was used as a reference, that was already performed to

parameterize the FF.³⁰ The experimental IR spectrum, the spectra computed from the MD simulation in polymer and in gas phase, and the QM reference are plotted Figure 11(a-d). The displacement vectors arising from the three most prominent peaks are drawn in Figure 12: as expected, the two lines at 802.7 and 1797.1 cm^{-1} correspond to the out-of-plane bending of the naphthalene hydrogens and to the C=O stretching; the mode at 1309.1 cm^{-1} involves an in-plane motion of the naphthalene hydrogens.

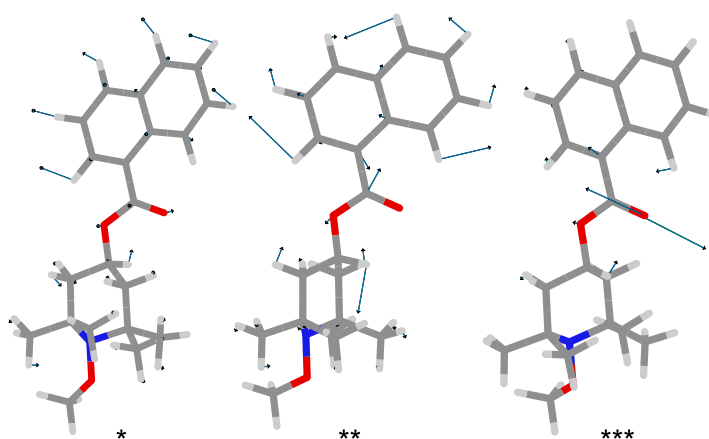


Figure 12: Displacement vectors relative to three relevant normal modes identified from the harmonic spectrum of the NfO-TEMPO-Me dye. The labels refer to the spectrum in Figure 11 (bottom): *: 802.7 cm^{-1} , **: 1309.1 cm^{-1} , ***: 1797.1 cm^{-1} .

The fair agreement, in term of wavenumbers, of the harmonic DFT-level spectrum and the MD based ones, could be easily predicted, since the simulations use a FF based on the DFT Hessian matrix. In this case, also the agreement with the experiment is good, though the lines may be shifted (*e.g.* the C=O band is translated by 80 cm^{-1}). On the other hand, as regards the peak intensities, the vibrational spectra calculated with the quantum corrected dipole ACF are in fairly good agreement with their experimental counterpart. It should be pointed out that the inclusion of anharmonicity in the FF definition, that is not present in the model employed here, could enhance the vibrational description of the system and lead to a more quantitative correspondence. Having said that, it can be underlined that the adoption of a specifically tailored FF allows for a rather reliable representation of the vibrational behavior of the dye. Since the present statistical determination of the dye's electronic spectra is based on configurations extracted from

classical MD simulations, the resulting spectrum will take into account the vibrational broadening with reasonable accuracy.

3.3.2 UV spectra

UV-Visible spectra were computed for the grafted dye, for both the absorption and emission bands, by averaging the TD-DFT signals from 100 snapshots extracted from the NPT simulations. The methodology, outlined in the Computational details, is similar to that used for toluene solution in Ref.,³⁰ thus the results are directly comparable.

For the “electronic embedding” (EE) calculations, the portion of polymer included explicitly is obtained by cutting a sphere of radius R_{cut} around the dye center of mass, and keeping the carbon atoms which lie inside along with the hydrogen atoms directly bonded to them. By doing this, the total charge of the MM explicit layer is zero. The choice of $R_{\text{cut}} = 14 \text{ \AA}$ is done for consistency with Ref.,³⁰ and is justified by the fact that the radial distribution function of the polymer around the dye, as well as for toluene, is almost equal to 1 at this distance (see Figures 4 and 13).

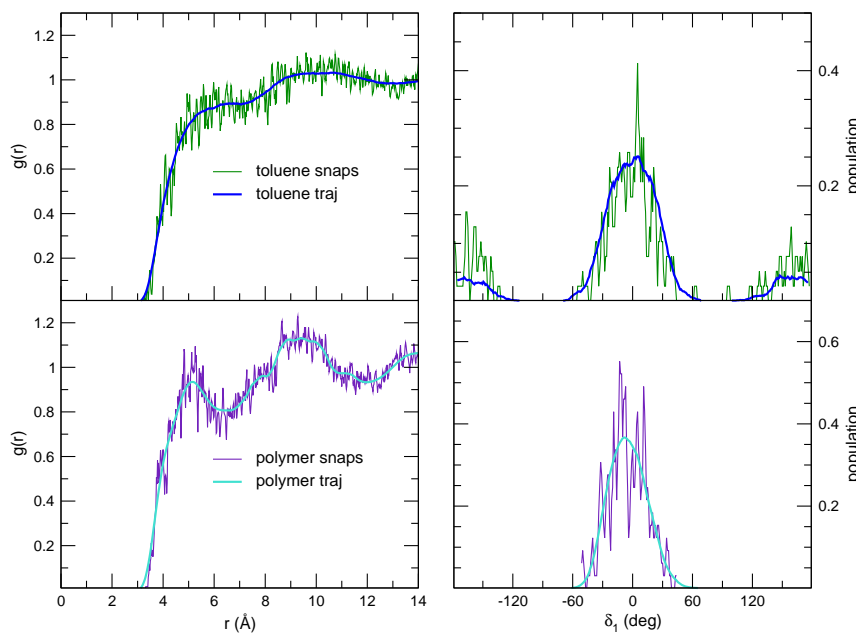


Figure 13: Pair correlation functions (left) and δ_1 dihedral distribution (right) for the NfO-TEMPO GS in the two considered embeddings, as calculated for the total trajectory (blue, indigo lines) and for the snapshots used for TD-DFT calculations (green, violet lines).

To substantiate the approach and to guarantee that the selection of equally spaced snapshots is not biased toward irrelevant configurations, some of the statistically generated curves that characterize the MD (*i.e.* solute-solvent pair distribution functions and δ_1 distribution) were plotted in Figure 13 taking into account the coordinates throughout the whole trajectory or only the ones corresponding to the selected snapshots. Although clearly noisy, the curves averaged only over the selected frames follow the trace of the more statistically sound black lines.

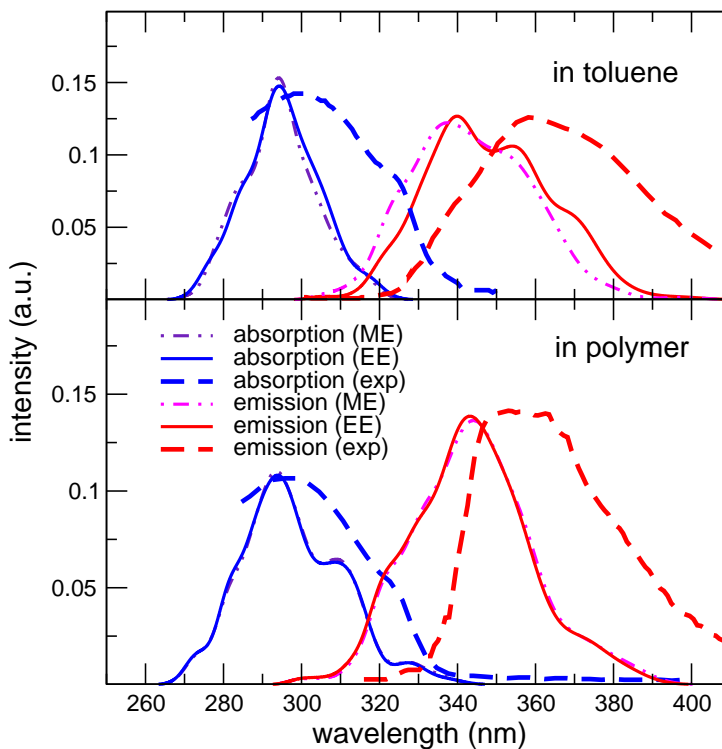


Figure 14: Absorption (indigo/blue lines) and emission spectra (magenta/red lines) of the NfO-TEMPO-Me dye in toluene solution (top, obtained in Ref. [30]), and of the NfO-TEMPO molecule covalently bonded to a polymer matrix (bottom, this work). The electronic transitions in both the embeddings are computed both in the GS and EES schemes. Experimental bands obtained in toluene solution and in polymer film, see Ref.[33] for details (dotted lines, arbitrarily rescaled in the Y axis) are reported for comparison.

The spectra that result from the statistical averaging are reported in Figure 14, lowest panel, and are compared to the same results (Ref.³⁰) obtained in toluene (top panel). In all cases, both ME and EE schemes were applied. It must be pointed out that the

chromophore is slightly different, since the methyl termination of NfO-TEMPO-Me is now substituted by a polymer carbon atom; however, the electronic transition takes place in the naphthoxy region which is unchanged. As far as the functionalized polyolefin absorption is concerned, ME (indigo, broken line) and EE (blue, solid) schemes converge to the same results, yielding a peak centered around 294 nm, which well compares to the absorption line (blue, dotted) obtained on a film of functionalized polyolefin, reported in Ref. [33] It may be worth noticing that the almost not distinguishable ME and EE band shape is a feature shared with the spectra computed in toluene, indicating that in both cases rather weak electrostatic interactions take place between the dye and the considered embeddings, that are not able to sensibly alter the absorption signal.

Turning to emission, the line peaked at 343 nm refers to the emission from the considered EES, computed in both schemes (magenta, broken line for ME and solid red for EE). Again the two approaches are almost indistinguishable. On the contrary the emission in toluene was found³⁰ more sensitive to electrostatic interactions, probably due to dispersion forces taking place between toluene's and naphthoxy aromatic rings. Within the polymer, the shape of the emission curve is entirely due to the "mechanical embedding", *i.e.* the effect of the polymer and its afore described cage on the conformations of the dye. The electrostatic role it plays in the electronic calculation is negligible: as it was remarked for the vibrational spectra, the apolar nature of the polymer suppress all the specific interactions that could lead to short-timescale or direct electrostatic effects.

By inspection of the line shapes, it can be observed that they well compare to the experimental ones, particularly when the broadening and the decay slope are considered. The experimental bulged decay of the absorption line at about 320 nm corresponds to a secondary peak, although overestimated and slightly shifted, in the computed spectrum ($\simeq 310$ nm). The computed emission line is found to be as broad as the reference one; moreover, the decay toward red loses the *plateau* observed in the solvated case ($\simeq 360 - 380$ nm exp.), as expected from the experimental spectra. Eventually, the experimental curve for longer wavelengths exhibits a shoulder at about 395 nm, that can be found also in the simulated spectrum at 370 nm. By looking at Table 2, the results, as concerns the peak wavelengths, are as good as found in the toluene case, when compared to the

System	Method	Absorption peak (nm)	Stokes shift (nm)
in toluene ^a	Computed	292	54
	Experim. ^b	299	62
in polymer	Computed	294	49
	Experim. ^b	296	62

Table 2: Values of the absorption wavelengths and of the Stokes shift, calculated at the line peaks, for the NfO-TEMPO dye in the considered environments. (a) Ref.,³⁰ (b) Ref.³³

experimental findings. In particular, the absorption peak is reproduced within 2 nm, while the error on the Stokes shift is of about 13 nm. By inspection of Figure 14, it appears that the main source of the latter difference is the blue shift of the computed signal with respect to the experimental emission line. As evidenced by the comparison between the two solvents, this shift is systematic and connected to the particular choice of the DFT functional/basis set combination, rather than to the embedding environment. For the Nfo-TEMPO chromophore, this issue has been addressed in detail in Ref. [30], where different functional/basis combinations were tested and the present choice was shown to best reproduce the experimental absorption line-shape.

4 Conclusions

A multi-layered protocol, rooted into classical MD simulations with accurate FFs and QM calculations, has been applied to investigate structural, dynamic and photophysical properties of a recently synthesized^{32,33} smart polymer, made by grafting the NfO-TEMPO dye onto an apolar PE matrix.

A specifically parameterized FF, previously³⁰ tailored to reproduce the NfO-TEMPO chromophore in its ground and excited states, was employed in MD simulations to account for the dye's behavior, whereas a refined set of literature parameters was employed to mimic the surrounding environment. A detailed analysis of the resulting trajectories revealed the existence of long lived cages, formed by the entangling polymer, around the dye, limiting both its rotational and librational dynamics. Conversely, the fast internal vibrations are found less affected by the surrounding polymer.

The reliability of this scenario was validated by the comparison of the computed IR and

UV-visible spectra with their experimental counterparts. The most important spectral signatures of the former were reproduced with good accuracy, for all considered environments, and the negligible effect of the embeddings on the dye's fast motions was confirmed by simulation. On the other hand, the different effects, experimentally registered, on the spectral broadening of the UV-visible spectra, were also reproduced, and their origin connected with the hindered dynamics within the polymer cages.

This work can be considered as a further advance in setting up a sound screening protocol, able to efficiently flank the experiment in the design of novel smart materials. For instance, future applications of the proposed procedure could help a better understanding of the different mechanisms subtending grafted and dispersed dyes, and their interaction with polymer matrices of increasing polarity. The conclusions that might be drawn from the comparison of such computational study, could be eventually exploited in the research of novel "smart" functionalized polymers. Work in this direction is currently in progress in our group,

5 Acknowledgements

This work has been supported by the Fondazione Cassa di Risparmio di Pisa under POLOPTEL project no. 167/09 and by the European Union's Seventh Framework Programme (FP7/2007-2013) under grant agreement No ERC-2012-AdG-320951-DREAMS. Partial funding was granted by the Italian Regione Toscana (Ricerca regionale in materia di salute, D.D. 3242-30/06/09). G.P. and S.M. are grateful to Dr. Elisa Passaglia for useful discussions and suggestions.

References

- [1] Zhang, Z.; Rehm, S.; Safont-Sempere, M.; Würthner, F. Vesicular Perylene Dye Nanocapsules As Supramolecular Fluorescent pH Sensor Systems, *Nature Chem.* **2009**, *1*, 623–629.
- [2] Sagara, Y.; Kato, T. Mechanically Induced Luminescence Changes In Molecular Assemblies, *Nature Chem.* **2009**, *1*, 605–610.

- [3] Sagara, Y.; Kato, T. Brightly Tricolored Mechanochromic Luminescence from a Single-Luminophore Liquid Crystal: Reversible Writing and Erasing of Images, *Angew. Chem. Int. Ed.* **2011**, *50*, 9128–9132.
- [4] Bredas, J.-L.; Marder, S. R.; Reichmanis, E. Preface to the Chemistry of Materials Special Issue on pi-Functional Materials, *Chem. Mater.* **2011**, *23*, 309.
- [5] Anzenbacher, P.; Li, F.; Palacios, M. A. Toward Wearable Sensors: Fluorescent Attoreactor Mats as Optically Encoded Cross-Reactive Sensor Arrays., *Angew. Chem. Int. Ed.* **2012**, *51*, 2345–2348.
- [6] Davis, D. A.; Hamilton, A.; Yang, J. L.; Cremer, L. D.; Van Gough, D.; Potisek, S. L.; Ong, M. T.; Braun, P. V.; Martinez, T. J.; White, S. R.; Moore, J. S.; Sottos N.R.. Force-Induced Activation of Covalent Bonds in Mechanoresponsive Polymeric Materials, *Nature* **2009**, *459*, 68–72.
- [7] Chen, Y.; Spiering, A.; Karthikeyan, S.; Peters, G.; Meijer, E.; Sijbesma, R. Mechanically Induced Chemiluminescence From Polymers Incorporating A 1,2-Dioxetane Unit In The Main Chain, *Nature Chem.* **2012**, *4*, 559–562.
- [8] Pucci, A.; Bizzarri, R.; Ruggeri, G. Polymer Composites With Smart Optical Properties, *Soft Matter* **2011**, *7*, 3689–3700.
- [9] Pucci, A.; Ruggeri, G. Mechanochromic Polymer Blends, *J. Mater. Chem.* **2011**, *21*, 8282–8291.
- [10] Ciardelli, F.; Ruggeri, G.; Pucci, A. Dye-Containing Polymers: Methods For Preparation Of Mechanochromic Materials, *Chem. Soc. Rev.* **2013**, *42*, 857–870.
- [11] Beiermann, A.; Kramer, S. L. B.; Moore, J. S.; White, S. R.; Sottos, N. R. Role of Mechanophore Orientation in Mechanochemical Reactions, *ACS Macro Lett.* **2012**, *1*, 163–166.
- [12] Yesodha, S. K.; Pillai, C. K. S.; Tsutsumi, N. Stable Polymeric Materials For Non-linear Optics: A Review Based On Azobenzene Systems, *Prog. Polym. Sci.* **2004**, *29*, 45–74.

- [13] Kumar, G. S.; Neckers, D. C. Photochemistry Of Azobenzene-Containing Polymers, *Chem. Rev.* **1989**, *89*, 1915–1925.
- [14] Natansohn, A.; Rochon, P. Photoinduced Motions In Azo-Containing Polymers, *Chem. Rev.* **2002**, *102*, 4139–4176.
- [15] Izumi, A.; Teraguchi, M.; Nomura, R.; Masuda, T. Synthesis Of Conjugated Polymers With Azobenzene Moieties In The Main Chain, *J. Polym. Sci. Polym. Chem.* **2000**, *38*, 1057–1063.
- [16] Alam, Z.; Shibahara, A.; Ogata, T.; Kurihara, S. Synthesis Of Azobenzene-Functionalized Star Polymers Via RAFT And Their Photoresponsive Properties, *Polymer* **2011**, *52*, 3696–3703.
- [17] Wang, D. H.; Lee, K. M.; Yu, Z.; Koerner, H.; Vaia, R. A.; White, T. J.; Tan, L. S. Photomechanical Response of Glassy Azobenzene Polyimide Networks, *Macromolecules* **2011**, *44*, 3840–3846.
- [18] Guillet, J. *Polymer Photophysics and Photochemistry*; Cambridge University Press: London, 1985.
- [19] Fox, M. A. *Photoinduced Electron Transfer*, edited by M. Chanon, Vol. A-D; Elsevier: Amsterdam, 1988.
- [20] Passaglia, E. ; Coiai, S. ; Cicogna, F. ; Ciardelli, F. Some recent advances in polyolefin functionalization, *Polymer International* **2014**, *63*, 12–21.
- [21] Chung, T.C.M. Functional Polyolefins for Energy Application, *Macromolecules* **2013**, *46*, 6671–6698.
- [22] Murugan, N. A.; Kongsted, J.; Rinkevicius, Z.; Ågren, H. Color Modeling Of Protein Optical Probes, *Phys. Chem. Chem. Phys.* **2012**, *14*, 1107–1112.
- [23] Murugan, N. A.; Apostolov, R.; Rinkevicius, Z.; Kongsted, J.; Lindahl, E.; Ågren, H. Association Dynamics and Linear and Nonlinear Optical Properties of an N-

- Acetyladanamide Probe in a POPC Membrane, *J. Am. Chem. Soc.* **2013**, *135*, 13590–13597.
- [24] Murugan, N. A.; Olsen, J. M. H.; Kongsted, J.; Rinkevicius, Z.; Aidas, K.; Ågren, H. Amyloid Fibril-Induced Structural and Spectral Modifications in the Thioflavin-T Optical Probe, *J. Phys. Chem. Lett.* **2013**, *4*, 70–77.
- [25] Mereau, R.; Castet, F.; Botek, E.; Champagne, B. Effect of the Dynamical Disorder on the Second-Order Nonlinear Optical Responses of Helicity-Encoded Polymer Strands, *J. Phys. Chem. A* **2009**, *113*, 6552–6554.
- [26] Fantacci, S.; Angelis, F. D.; Sgamellotti, A.; Marrone, A.; Re, N. Photophysical Properties of [Ru(phen)₂(dppz)]²⁺ Intercalated into DNA: An Integrated CarParrinello and TDDFT Study, *J. Am. Chem. Soc.* **2005**, *127*, 14144–14145.
- [27] Sanna, N.; Chillemi, G.; Gontrani, L.; Grandi, A.; Mancini, G.; Castelli, S.; Zagotto, G.; Zazza, C.; Barone, V.; Desideri, A. UV-Vis Spectra Of The Anticancer Camptothecin Family Drugs In Aqueous Solution: Specific Spectroscopic Signatures Unraveled By A Combined Computational And Experimental Study, *J. Phys. Chem. B* **2009**, *113*, 5369–5375.
- [28] Barone, V.; Bloino, J.; Biczysko, M.; Santoro, F. Fully Integrated Approach to Compute Vibrationally Resolved Optical Spectra: From Small Molecules to Macrosystems, *J. Chem. Theory Comput.* **2009**, *5*, 540–554.
- [29] Bloino, J.; Biczysko, M.; Santoro, F.; Barone, V. General Approach to Compute Vibrationally Resolved One-Photon Electronic Spectra, *J. Chem. Theory Comput.* **2010**, *6*, 1256–1274.
- [30] De Mitri, N.; Monti, S.; Prampolini, G.; Barone, V. Absorption and Emission Spectra of a Flexible Dye in Solution: A Computational Time-Dependent Approach, *J. Chem. Theory Comput.* **2013**, *9*, 4507–4516.
- [31] Prampolini, G.; Bellina, F.; Biczysko, M.; Cappelli, C.; Carta, L.; Lessi, M.; Pucci, A.; Ruggeri, G.; Barone, V. Computational Design, Synthesis, And Mechanochromic

- Properties Of New Thiophene-Based π -Conjugated Chromophores., *Chem. Eur. J* **2013**, *19*(6), 1996–2004.
- [32] Cicogna, F.; Coiai, S.; Passaglia, E.; Tucci, I.; Ricci, L.; Ciardelli, F.; Batistini, A. Grafting Of Functional Nitroxyl Free Radicals To Polyolefins As A Tool To Postreactor Modification Of Polyethylene-Based Materials With Control Of Macromolecular Architecture, *J. Polym. Science. A* **2011**, *49*, 781–795.
- [33] Cicogna, F.; Coiai, S.; Pinzino, C.; Ciardelli, F.; Passaglia, E. Fluorescent Polyolefins By Free Radical Post-Reactor Modification With Functional Nitroxides, *React. Func. Polym.* **2012**, *72*, 695–702.
- [34] Prampolini, G.; Monti, S.; De Mitri, N.; Barone, V. Evidences of long lived cages in functionalized polymers: Effects on chromophore dynamic and spectroscopic properties, *Chem. Phys. Lett.* **2014**, *601*, 134–138.
- [35] Ha, T.; Enderle, T.; Chemla, D. S.; R.Selvin, P.; Weiss, S. Quantum Jumps Of Single Molecules At Room Temperature, *Chem. Phys. Lett.* **1997**, *271*, 1–5.
- [36] Dickson, R. M.; Cubitt, A. B.; Tsien, R. Y.; Moerner, W. E. On/Off Blinking And Switching Behaviour Of Single Molecules Of Green Fluorescent Protein, *Nature* **1997**, *388*, 355–358.
- [37] Weston, K. D.; Carson, P. J.; Metiu, H.; Buratto, S. K. Room-Temperature Fluorescence Characteristics Of Single Dye Molecules Adsorbed On A Glass Surface, *J. Chem. Phys.* **1998**, *109*, 7474–7485.
- [38] Lu, H. P.; Xie, X. S. Single-Molecule Spectral Fluctuations At Room Temperature, *Nature* **1997**, *385*, 143–146.
- [39] Ying, L. M.; Xie, X. S. Fluorescence Spectroscopy, Exciton Dynamics, And Photochemistry Of Single Allophycocyanin Trimers, *J. Phys. Chem. B* **1998**, *102*, 10399–10409.
- [40] Veerman, J. A.; Garcia-Parajo, M. F.; Kuipers, L.; van Hulst, N. F. Time-Varying Triplet State Lifetimes of Single Molecules, *Phys. Rev. Lett.* **1999**, *83*, 2155–2158.

- [41] Weston, K. D.; Carson, P. J.; DeAro, J. A.; Buratto, S. K. Single-Molecule Detection Fluorescence Of Surface-Bound Species In Vacuum, *Chem. Phys. Lett.* **1999**, *308*, 58–64.
- [42] Cacelli, I.; Prampolini, G. Parametrization and Validation of Intramolecular Force Fields Derived from DFT Calculations, *J. Chem. Theory Comput.* **2007**, *3*, 1803–1817.
- [43] Barone, V.; Cacelli, I.; De Mitri, N.; Licari, D.; Monti, S.; Prampolini, G. Joyce And Ulysses: Integrated And User-Friendly Tools For The Parameterization Of Intramolecular Force Fields From Quantum Mechanical Data, *Phys. Chem. Chem. Phys.* **2013**, *15*, 3736–3751.
- [44] Jorgensen, W.; Maxwell, D.; Tirado-Rives, J. Development and Testing of the OPLS All-Atom Force Field on Conformational Energetics and Properties of Organic Liquids, *J. Am. Chem. Soc.* **1996**, *118*, 11225–11236.
- [45] Case, D. A.; Cheatham, T.; Darden, T.; Gohlke, H.; Luo, R.; Jr.", K. M. M.; Onufriev, A.; Simmerling, C.; Wang, B.; Woods, R. The Amber Biomolecular Simulation Programs, *J. Computat. Chem.* **2005**, *26*, 1668–1688.
- [46] Martienssen, W., Warlimont, H., Eds. *Springer Handbook of Condensed Matter and Materials Data*; Springer: Berlin, 2005.
- [47] Brent Strong, A. *Plastics: Materials and Processing*; Prentice Hall: Upper Saddle River, New Jersey, 2000.
- [48] Murzyn, K.; Bratek, M.; Pasenkiewicz-Gierula, M. Refined OPLS All-Atom Force Field Parameters for n-Pentadecane, Methyl Acetate, and Dimethyl Phosphate., *J. Phys. Chem. B* **2013**, *117*, 16388–96.
- [49] Tiberio, G.; Muccioli, L.; Berardi, R.; Zannoni, C. Towards In Silico Liquid Crystals. Realistic Transition Temperatures And Physical Properties For n-Cyanobiphenyls Via Molecular Dynamics Simulations., *ChemPhysChem.* **2009**, *10*, 125–36.

- [50] van der Spoel, D.; Lindahl, E.; Hess, B.; van Buuren, A. R.; Apol, E.; Meulenhoff, P.; Tieleman, D.; Sijbers, A.; Feenstra, K.; van Drunen, R.; Berendsen, H. *GROMACS4.5*; Gromacs User Manual version 4.5.4: www.gromacs.org, 2010.
- [51] Berendsen, H. J. C.; Postma, J. P. M.; van Gunsteren, W.; Di Nola, A.; Haak, J. R. Molecular Dynamics With Coupling To An External Bath, *J. Chem. Phys.* **1984**, *81*, 3684–3690.
- [52] McQuarrie, D. *Statistical Thermodynamics*; University Science Books: Mill Valley, CA, 1973.
- [53] Schofield, P. Space-Time Correlation Function Formalism for Slow Neutron Scattering, *Phys. Rev. Lett.* **1960**, *4*, 239–240.
- [54] Ramírez, R.; López-Ciudad, T.; Kumar P, P.; Marx, D. Quantum Corrections To Classical Time-Correlation Functions: Hydrogen Bonding And Anharmonic Floppy Modes, *The Journal of Chemical Physics* **2004**, *121*(9), 3973–3983.
- [55] Egorov, S.; Skinner, J. Semiclassical Approximations To Quantum Time Correlation Functions, *Chemical Physics Letters* **1998**, *293*(56), 469–476.
- [56] Barone, V.; Cimino, P. Accurate And Feasible Computations Of Structural And Magnetic Properties Of Large Free Radicals: The PBE0/N07D Model, *Chem. Phys. Lett.* **2008**, *454*(13), 139–143.
- [57] Gaussian09, Revision C.01. Frisch, M. J.; Trucks, G. W.; Schlegel, H. B.; Scuseria, G. E.; Robb, M. A.; Cheeseman, J. R.; Scalmani, G.; Barone, V.; Mennucci, B.; Petersson, G.; Nakatsuji, H.; Caricato, M.; Li, X.; Hratchian, H. P.; Izmaylov, A. F.; Bloino, J.; Zheng, G.; Sonnenberg, J. L.; Hada, M.; Ehara, M.; Toyota, K.; Fukuda, R.; Hasegawa, J.; Ishida, M.; Nakajima, T.; Honda, Y.; Kitao, O.; Nakai, H.; Vreven, T.; Montgomery, J. A.; Peralta, J. E.; Ogliaro, F.; Bearpark, M.; Heyd, J. J.; Brothers, E.; Kudin, K. N.; Staroverov, V. N.; Kobayashi, R.; Normand, J.; Raghavachari, K.; Rendell, A.; Burant, J.; Iyengar, S. S.; Tomasi, J.; .; Cossi, M.; Rega, N.; Millam, J. M.; Klene, M.; Knox, J. E.; Cross, J. B.; Bakken, V.; Adamo, C.; Jaramillo, J.;

- Gomperts, R.; Stratmann, R. E.; Yazyev, O.; Austin, A. J.; Cammi, R.; Pomelli, C.; Ochterski, J. W.; Martin, R. L.; Morokuma, K.; Zakrzewski, V. G.; Voth, G. A.; Salvador, P.; Dannenberg, J. J.; Dapprich, S.; Parandekar, P. V.; Mayhall, N. J.; Daniels, A. D.; Farkas, O.; Foresman, J. B.; Ortiz, J. V.; Cioslowski, J.; Fo, D. J.; Gaussian, Inc., Wallingford CT, **2009**.
- [58] Monti, S.; Cicogna, F.; Passaglia, E.; Prampolini, G.; Barone, V. Theoretical Study Of The Conformational And Optical Properties Of A Fluorescent Dye. A Step Toward Modeling Sensors Grafted On Polymer Structures., *Phys. Chem. Chem. Phys.* **2011**, *13*, 21471–8.
- [59] Li, J.; Wang, I.; Fruchey, K.; Fayer, M. D. Dynamics in Supercooled Ionic Organic Liquids and Mode Coupling Theory Analysis, *J. Phys. Chem. A* **2006**, *110*, 10384–10391.
- [60] Affouard, F.; Descamps, M. Is There Something of Mode Coupling Theory in Orientationally Disordered Crystals?, *Phys. Rev. Lett.* **2001**, *87*, 035501–035504.
- [61] Bordat, P.; Lerbret, A.; Descamps, M.; Affourad, F. Slow Dynamics In Glass-Forming Materials, *Molecular Simulation* **2006**, *32*, 1057–1068.
- [62] Ricker, M.; Affourad, F.; Schilling, R.; M.Descamps. Glassy Behavior of Molecular Crystals: A Comparison Between Results from MD-simulation and Mode Coupling Theory, *J. Non-Cryst. Solids* **2006**, *352*, 4814.
- [63] De Gaetani, L.; Prampolini, G.; Tani, A. Anomalous Diffusion and Cage Effects in the Isotropic Phase of a Liquid Crystal, *J. Phys. Chem. B* **2007**, *111*, 7473–7477.
- [64] De Gaetani, L.; Prampolini, G.; Tani, A. Subdiffusive Dynamics Of A Liquid Crystal In The Isotropic Phase, *J. Chem. Phys.* **2008**, *128*, 194501.
- [65] Colmenero, J.; Alvarez, F.; Arbe, A. Self-Motion And The α -Relaxation In A Simulated Glass-Forming Polymer: Crossover From Gaussian To Non-Gaussian Dynamic Behavior, *Phys. Rev. E* **2002**, *65*, 041804–041815.

- [66] Binder, K.; Baschnagel, J.; Paul, W. Glass Transition Of Polymer Melts: Test Of Theoretical Concepts By Computer Simulation, *Prog. Polym. Sci* **2003**, *28*, 115–172.
- [67] Paul, W.; Smith, G. D. Structure And Dynamics Of Amorphous Polymers: Computer Simulations Compared To Experiment And Theory, *Rep. Prog. Phys.* **2004**, *67*, 1117–1186.